FACTA UNIVERSITATIS
Series: **Electronics and Energetics** Vol. 39, N° 1, March 2026, pp. 257 - 268
https://doi.org/10.2298/FUEE2601257S

Original scientific paper

HIGH-VOLTAGE SURGE IMPACT ON THICK-FILM SENSORS FOR STRUCTURAL HEALTH MONITORING: RESISTANCE AND NOISE SPECTROSCOPY ANALYSIS

Zdravko Stanimirović[1], Ana Stanimirović[2], Aleksandar Savić[3], Ivanka Stanimirović[1]

[1]"Vinča" Institute of Nuclear Sciences - National Institute of the Republic of Serbia, University of Belgrade, Serbia
[2]Faculty of Physics, University of Belgrade, Serbia
[3]Faculty of Civil Engineering, University of Belgrade, Serbia

ORCID iDs:	Zdravko Stanimirović	https://orcid.org/0000-0002-2048-0027
	Ana Stanimirović	https://orcid.org/0009-0002-6002-7347
	Aleksandar Savić	https://orcid.org/0000-0002-1777-6775
	Ivanka Stanimirović	https://orcid.org/0000-0003-2445-611X

Abstract. *This study explores the effects of high-voltage electrical surges on the performance and structural integrity of thick-film strain sensors developed for structural health monitoring in steel infrastructure. The sensors were fabricated using screen-printing techniques with a bismuth lead ruthenate-based resistive composition deposited on alumina ceramic substrates. To simulate realistic operational conditions, the sensors were mounted on steel beams and subjected to four-point bending to induce mechanical strain. Following mechanical loading, controlled high-voltage surge pulses were applied to emulate extreme electrical events. Sensor response was characterized before and after surge exposure using both static resistance measurements and current noise spectral analysis. While resistance measurements showed limited change, noise spectroscopy revealed microstructural damage undetectable by conventional means. The findings highlight the degradation mechanisms arising from electromechanical stress and demonstrate the effectiveness of noise spectroscopy as a non-destructive diagnostic tool. These results support the use of thick-film sensors in electrically demanding environments.*

Key words: *thick-film strain sensors, structural health monitoring, high-voltage surge testing, low-frequency noise, tunnelling conduction, metal-insulator-metal junctions*

Received June 10, 2025; revised August 20, 2025; accepted September 16, 2025
Corresponding author: Ivanka Stanimirović
"Vinča" Institute of Nuclear Sciences – National Institute of the Republic of Serbia, University of Belgrade.
E-mail: ivanka.stanimirovic@vin.bg.ac.rs

1. INTRODUCTION

Throughout their operational lifespan, civil engineering structures endure gradual deterioration and exposure to diverse environmental challenges, such as seismic disturbances, hydrodynamic forces, soil shifts and extreme climatic conditions. As infrastructure becomes increasingly complex and expansive, the deployment of sophisticated structural health monitoring (SHM) systems is imperative to uphold structural integrity, enhance safety and refine maintenance strategies. SHM functions on the principle that a structure's mechanical and material properties change over time due to external forces, wear, corrosion and other degradation processes. By persistently tracking strain variations, internal stress fluctuations and additional crucial metrics, early indicators of structural damage can be identified, helping to prevent catastrophic failures [1-3]. Strain measurement is especially vital in SHM, offering essential insights into load distribution, fatigue endurance and the prolonged functionality of civil infrastructure.

Various sensor technologies have been explored for strain measurement in SHM, including metal foil strain gauges, fiber optic sensors and piezoelectric sensors, each possessing unique benefits and limitations [4-9]. In recent years, thick-film strain sensors have gained prominence as a resilient and cost-effective alternative for SHM applications, delivering an optimal balance of mechanical strength, environmental resistance and seamless integration. Unlike conventional strain gauges that rely on adhesive attachment, thick-film strain sensors feature screen-printed resistive films sintered onto various substrates, which ensures strong adhesion, durability and resistance to mechanical fatigue [10-12]. These sensors exhibit remarkable thermal stability, with minimal resistance fluctuations across diverse operational environments, making them highly suitable for outdoor structures subjected to varying temperatures. Furthermore, thick-film strain sensors must demonstrate resilience against high-voltage surges, a crucial attribute for steel components in modern glass-steel constructions, bridges and critical infrastructure that face risks from lightning strikes and electrical disturbances. The differences in electrical and thermal performance between thick-film and other SHM sensor technologies are highlighted in Table 1.

This research examines the behavior of screen-printed $Bi_2Ru_2O_7$-based ceramic strain sensors affixed to steel bars under high-voltage surge conditions. To analyze the influence of high-voltage surges, this study measures resistance variations in the sensors and investigates how structural changes correlate with noise performances. By assessing these interactions, the research provides a deeper understanding of how high-voltage exposure impacts sensor functionality. The findings highlight the promise of thick-film technology as a reliable and scalable solution for SHM, demonstrating superior durability and adaptability compared to conventional strain sensing techniques. Implementing thick-film sensors within civil infrastructure can bolster predictive maintenance efforts, lower upkeep costs and extend the operational lifespan of essential structures. This research contributes to the evolution of SHM methodologies, offering key insights into the feasibility of thick-film strain sensors in high-voltage environments.

Table 1 Characteristics of thick-film sensors, metal foil strain gauges, fiber optic sensors and piezoelectric sensors for SHM [13]

Sensor Type	Thick-Film Sensors	Metal Foil Strain Gauges	Fiber Optic Sensors	Piezoelectric Sensors
GF	2–35	~2	0.8–1.2	Varies
TCR (ppm/°C)	±50 to ±200	±5 to ±20	~0	Varies

2. Experimental Evaluation of High-Voltage Surge Effects on Thick-Film Strain Sensors

To assess the effects of high-voltage surges on thick-film strain sensors for structural health monitoring, thick-film strain sensors were affixed to steel bars (Fig. 1a). The sensors were fabricated on 0.635 mm thick alumina (96% Al_2O_3) substrates, combined with a $Bi_2Ru_2O_7$-based thick-film resistive composition exhibiting a sheet resistance of 10 kΩ/sq. The resistive film was applied using standard screen-printing techniques with a semiautomatic screen printer. A stainless-steel screen, stretched over an aluminum frame, was employed to transfer the thick-film composition onto the substrate. The printed layer pattern was defined by a 200-mesh stainless-steel screen with emulsion thicknesses of 10-12 μm, ensuring high-resolution deposition of the resistive film. A Pd/Ag conductive thick film was employed for the fabrication of contact pads to ensure reliable electrical connections in SHM applications. Each sensor, measuring 3 × 21 mm², was segmented into seven 3 × 3 mm² sections, separated by six contact pads (Fig. 1a). Following deposition, the printed resistive layers underwent a series of precisely controlled curing and firing steps to ensure stable electrical characteristics.

The curing process involved initial leveling at room temperature, followed by drying at 150 °C for 10 minutes in an infrared conveyor dryer. Subsequently, the resistive layers, with a thickness of 25 ± 3 μm, were subjected to a firing cycle lasting 60 minutes, including a 10-minute dwell time at a peak temperature of 850 °C. The conductive layers underwent a separate firing process lasting 30 minutes at the same peak temperature to ensure optimal adhesion and conductivity.

Thick-film strain sensors were attached to steel bars, commonly used as reinforcement in concrete structures and as load-bearing elements in bridges, high-rise buildings and tunnels, where precise strain monitoring is critical for structural integrity [14-15]. The mechanical properties of $Bi_2Ru_2O_7$-based thick-film strain sensors are well-matched with the modulus of elasticity of steel (210 GPa [16]), enabling accurate strain measurements while minimizing material incompatibilities. Moreover, screen-printed thick-film sensors on alumina substrates exhibit high mechanical strength, with an elasticity modulus of 300–400 GPa [17], making them more compatible with steel than with concrete (elasticity modulus of 10–30 GPa [18]). This compatibility renders them particularly suitable for direct application on exposed steel components in modern glass-steel constructions, bridges and critical infrastructure.

All sensor samples were fabricated at the Institute for Electronics and Telecommunications IRITEL a.d. Beograd, Serbia. Resistance measurements were conducted using the National Instruments VB-8034 Virtual Bench Instrument to ensure precise and reliable data acquisition under various strain conditions. The response of the ceramic strain sensors to high-voltage surges was systematically evaluated using a Haefely P6T pulse generator, capable of delivering 10/700 μs pulses to simulate rapid electrical transients commonly encountered in structural environments (Fig. 1b). A four-point bending test, designed to apply maximum flexural stress between two loading points, was performed at the Faculty of Civil Engineering, University of Belgrade. The steel bars used had dimensions of 200 × 20 × 40 mm, with a support span of 180 mm and a distance between loading points of 100 mm. This configuration ensures uniform strain distribution along the specimen length, providing realistic simulation of strain conditions in steel structural elements used in SHM (Fig. 1a). The rate of loading was not controlled, as the experimental setup required fine

manual adjustment to achieve the target substrate deflection. To prevent sensor detachment, substrate deflection was set to 300 μm, selected based on the breaking point of the alumina substrate determined during preliminary three-point bending tests and the properties of the adhesive used to attach the sensor to the steel bar.

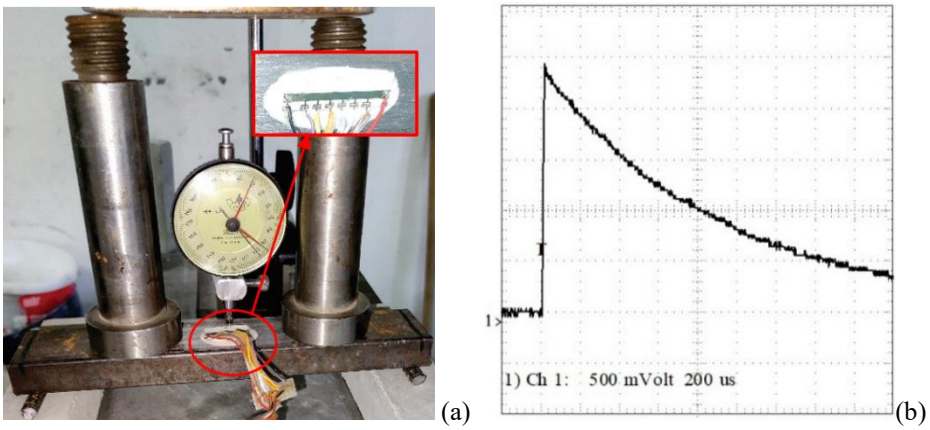

(a) (b)

Fig. 1 (a) Thick-film strain sensor attached to a steel bar undergoing a four-point bending test and (b) 10/700 μs pulse delivered by Haefely P6T pulse generator

The electrical straining conditions were carefully controlled to facilitate gradual resistance variations during pulse application. The sensors were subjected to pulse increments of 250 V, ranging from 3 kV to 5.25 kV, with the generator's output resistance fixed at 25 Ω. The testing procedure began with ten pulses applied at a frequency of six pulses per minute, with the voltage gradually increased from 3 kV to 5 kV. Subsequently, four single pulses with a peak amplitude of 5.25 kV were introduced. Throughout the testing process, gauge factor (*GF*) values were continuously monitored to evaluate the sensor response. The high-voltage surge testing adhered strictly to ITU-T K.20, the industry standard for thick-film surge resistor evaluation, ensuring the validity and applicability of the findings for assessing the performance of thick-film strain sensors in SHM applications. Current noise spectra before and after high-voltage surge testing were measured using a Keithley Model 103A nanovolt amplifier in conjunction with an HP-3561B Dynamic Signal Analyzer over a frequency range of 10 Hz to 10 kHz. All measurements were conducted under controlled conditions at room temperature (T=295 K) to ensure consistency and accuracy in the acquired data. Experimental arrangement employed in the characterization of the thick-film strain sensor is presented in Figure 2.

3. ANALYSIS OF THE EFFECTS OF HIGH-VOLTAGE SURGES ON THICK-FILM STRAIN SENSORS

During the experimental procedure, the sensors were exposed to a controlled sequence of high-voltage pulses to evaluate their electrical stability and resistance behavior under increasing electrical stress. The applied voltage was incrementally raised in 250 V steps, ranging from an initial 3 kV to a maximum of 5.25 kV. The testing procedure started with ten pulses delivered at a frequency of six pulses per minute, with the voltage steadily rising

from 3 kV to 5 kV. As the applied voltage increased, a gradual decrease in resistance was recorded, suggesting an alteration in the sensor's conductive pathways due to electrical stress. Once resistance variations approached a threshold of approximately 3 %, the pulse frequency was reduced to a single pulse per voltage increment to allow for precise tracking of further resistance fluctuations. Interestingly, at that point resistance values exhibited stabilization, indicating the sensor's capacity to reach an electrically stable state despite prolonged exposure to high-voltage transients. Additionally, the gauge factor measurements remained consistent throughout the experiment, confirming that the sensor maintained its strain sensitivity and overall functional integrity despite the imposed electrical stress conditions. The effects of high-voltage surges on the resistance and gauge factor of thick-film strain sensors at a substrate deflection of 300 μm are presented in Fig. 3. Data are presented for two sensors with initial resistances of R_1=33.84 kΩ and R_2=31.94 kΩ, highlighting resistance variations and gauge factor stability under electrical stress.

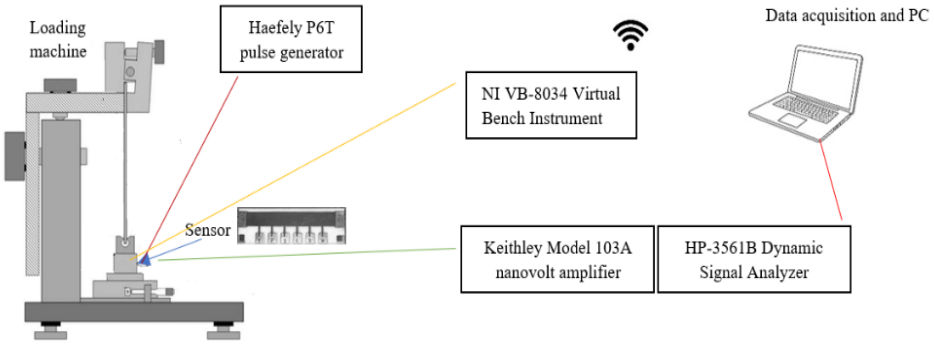

Fig. 2 Experimental arrangement employed in the characterization of the thick-film strain sensor

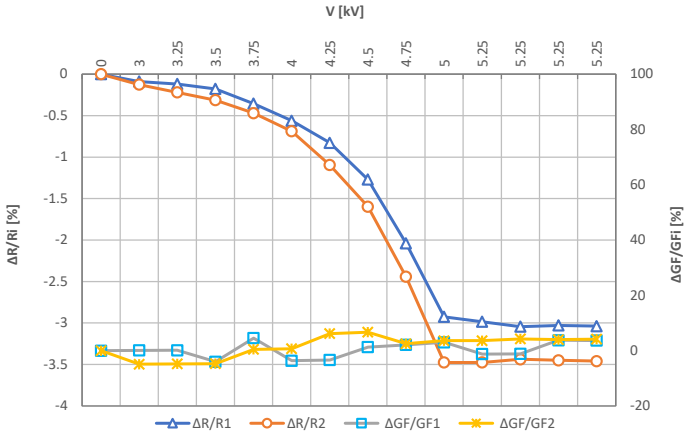

Fig. 3 Effect of high-voltage surges on the resistance and gauge factor of two thick-film strain sensors at a substrate deflection of 300 μm

The electrical conduction in thick-film resistive materials is governed by a combination of contact conduction and tunneling conduction mechanisms [19]. The resistive film comprises numerous parallel conducting chains, where adjacent conductive particles are either in direct contact or separated by thin layers of borosilicate glass. Under these conditions, the overall resistance of the film can be expressed as:

$$R = \frac{K_c}{M^2} R_c + \frac{K_b}{M^2} R_b \tag{1}$$

where Rc represents the contact resistance between neighboring conductive particles, R_b denotes the barrier resistance associated with tunneling through the insulating borosilicate glass layer, M is the total number of parallel conducting chains within the thick-film resistive network, K_c is the number of direct contacts between adjacent particles and K_b corresponds to the number of metal-insulator-metal (MIM) junctions formed by conductive particles separated by the insulating glass phase. In this context, the total number of electrical junctions between adjacent conducting particles, K, can be expressed as:

$$K = K_c + K_b \tag{2}$$

To systematically investigate the effects of applied strain on conduction pathways - particularly the transitions between direct interparticle contact and the formation or breakdown of MIM junctions - the relative contributions of contact resistance and barrier resistance can be introduced as [20]:

$$p = \frac{K_c}{K} \tag{3}$$

$$1 - p = \frac{K_b}{K} \tag{4}$$

Where p represents the fraction of conductive pathways governed by direct particle-to-particle contact, while $1\text{-}p$ corresponds to the proportion of conduction occurring via tunneling through MIM junctions. These parameters provide a framework for analyzing strain-induced modifications in the thick resistive film.

If we define thick resistive films conductance as:

$$G = \frac{M^2}{K[pR_c + (1-p)R_b]} \tag{5}$$

Considering the volume fraction of the conductive phase within the resistive film composition and the inherent relationship $R_c << R_b$, for low-ohmic formulations the overall conductance can be approximated as:

$$G \approx \frac{M^2}{pKR_c} \tag{6}$$

For high-ohmic compositions, where tunneling conduction through the MIM junctions dominates, the conductance is given by:

$$G \approx \frac{M^2}{(1-p)KR_b} \tag{7}$$

These expressions highlight the dependence of conductance on the proportion of direct contact pathways and MIM-mediated conduction, providing insight into the resistive film's behavior under varying electrical and mechanical conditions.

The experimental data presented in Fig. 2 demonstrate an initial reduction in resistance during high-voltage surge testing of strained thick-film sensors at a substrate deflection of 300 μm. For low-ohmic formulations, as described by Eq. (6), the parameter p decreases, indicating a reduction in the number of direct conductive contacts between neighboring particles. Consequently, in low-ohmic compositions, the dominant conduction mechanism transitions from contact-based conduction to tunneling conduction through MIM junctions. Conversely, in high-ohmic formulations, as described by Eq. (7), the parameter p increases, signifying a greater number of conductive contacts between adjacent particles. As a result, in high-ohmic compositions, the predominant conduction mechanism shifts from tunneling conduction to direct contact conduction.

Following the initial decrease in resistance, the resistance values reached a stable state, demonstrating the sensor's ability to attain electrical equilibrium despite sustained exposure to high-voltage transients. Throughout the experimental procedure, the gauge factor remained invariant, indicating that the sensor preserved its strain sensitivity and functional reliability under the applied electrical stress conditions.

Figure 4 illustrates the contribution of contact resistances (p) for the thick-film strain sensors characterized in Figure 2. The calculations were performed using the following parameter values: M=2.8·10^5, K=2.7·10^9, K_c=9.0541·10^8, K_b=1.81·10^9, R_c=136.97 Ω, R_b=1.34·10^7 Ω, corresponding to a 10 kΩ/sq thick-film resistor formulation. This particular composition was selected due to its intermediate electrical characteristics, encompassing attributes of both low-ohmic and high-ohmic resistive materials. The observed initial decrease in resistance, accompanied by a corresponding increase in p, suggests that tunneling conduction mechanisms play a dominant role in the early stages of high-voltage surge exposure.

Considering that low-frequency noise sources in thick-film resistors are closely related to conduction mechanisms, measurements of the current noise spectrum were performed for different current levels before and after high-voltage surge testing. Noise sources include fluctuations in contact resistance and intrinsic particle resistance in the case of conduction through conductive particles and their interconnections, as well as noise arising from Nyquist noise modulation and fluctuations caused by trap states in glass barriers when conduction occurs through these barriers [21]. The results, depicted in Fig. 5, correspond to a thick-film strain sensor with an initial resistance of R_2=31.94 kΩ.

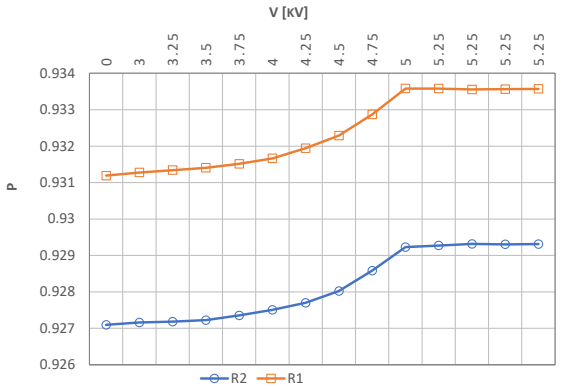

Fig. 4 Contribution of contact resistances p for two sensors with initial resistances of R_1=33.84 kΩ and R_2=31.94 kΩ

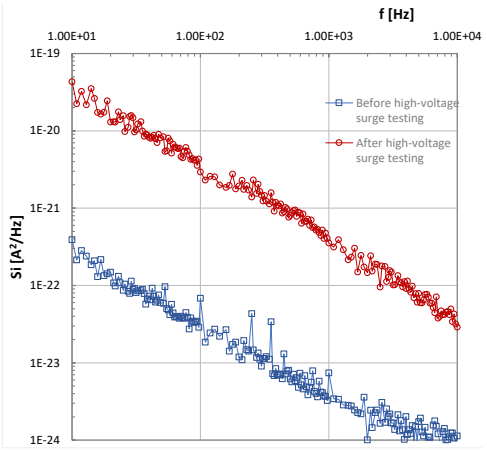

Fig. 5 Current noise spectrum measured before and afterhigh-voltage surge testing of strained thick-film strain sensor with an initial resistance R_2=31.94 kΩ

In the context of low-frequency noise, assuming that noise originating from fluctuations within the MIM junction is the dominant contribution to the overall noise, the relative voltage noise spectrum can be expressed as [21]:

$$\frac{S_V(f)}{V^2} \approx \frac{1}{K(1-p)\left(1+\frac{pR_C}{(1-p)R_b}\right)^2} \cdot \frac{S_{VBN}(f)}{V_B^2} + \frac{K_t}{K^2(1-p)^2\left(1+\frac{pR_C}{(1-p)R_b}\right)^2} \cdot \frac{S_{VT}(f)}{V_B^2} \tag{8}$$

where $S_{VBN}(f)/V_B^2$ represents the relative voltage noise spectrum resulting from Nyquist noise modulation and $S_{VT}(f)/V_B^2$ corresponds to the relative voltage noise spectrum attributed to the presence of traps within the glass barriers. When metallic conduction is the primary source of low-frequency noise [21]:

$$\frac{S_V(f)}{V^2} \approx \frac{1}{Kp\left(1+\frac{(1-p)R_b}{pR_C}\right)^2} \cdot \frac{S_{VC}(f)}{V_C^2} \tag{9}$$

To gain a more comprehensive understanding of the contribution of each low-frequency noise source to the total noise spectra before and after high-voltage surge testing, a fitting procedure was conducted using the experimental data presented in Fig. 4 and the following theoretical expression:

$$S_I(f) = A + \frac{B}{f^\gamma} + \sum_i \frac{C_i}{2\pi f_{Ci}\left(1+\frac{f^2}{f_{Ci}^2}\right)} \tag{10}$$

with the first term representing thermal noise:

$$A = 4kTR \tag{11}$$

where k is the Boltzmann constant, T is the absolute temperature and R is the resistance of the thick resistive film. The second term corresponds to *1/f* noise with parameters B and γ, while the third term represents the sum of noise spectra of Lorentzian shape, characterized by parameters C_i and characteristic frequencies f_{Ci}.

The fitting results corresponding to the data presented in Fig. 5, along with the individual contributions of various noise sources to the total current noise spectrum, are shown in Figs. 6a and 6b for strained thick-film strain sensor with an initial resistance of R_2=31.94 kΩ, both before and after high-voltage testing. As can be seen from Fig. 6a, the total current noise spectrum of the mechanically strained sensor exhibits both *1/f* and thermal noise. The *1/f* noise is composed of several contributions: fluctuations of contact resistances and the resistances of individual conducting particles within the conduction network, fluctuations in potential barrier heights due to Nyquist noise in the glassy matrix and fluctuations in the occupancy of charge carrier traps. Under the applied mechanical straining, the dominant contribution arises from fluctuations in barrier widths, as the number of conduction chains, contacts, and barrier heights remain largely unaffected by strain.

The results obtained from current noise spectrum measurements following high-voltage surge testing indicate that the current noise spectrum increases as a consequence of electrical stress. Interpreted through the noise index parameter p, this increase implies a decrease in p, according to Eqs. 8 and 9. However, this behavior is not consistent with the p values derived from resistance measurements shown in Fig. 3. Having in mind that the applied model excludes possibility of change in noise values for two neighboring conducting particles and MIM junctions, as well as value variations for contact and barrier resistances due to straining, noise performances of stained resistors could be explained using redistribution of numbers of contacts and MIM junctions as well as adequate contributions of noise due to metallic conduction and noise due to fluctuations in MIM junctions to total noise of strained resistor. This is in accordance with results shown in Fig. 6b. The total current noise spectrum is dominated by *1/f* noise, arising from fluctuations in potential barrier heights due to Nyquist noise within the glassy matrix [22-23] and fluctuations in the occupancy of charge carrier traps. In addition to the dominant *1/f* noise, a significant contribution to the spectrum originates from three Lorentzian components. The Lorentzian components observed in the low-frequency noise spectrum arise from traps located within the insulating layers of metal–insulator–metal (MIM) structures [24]. A trap may be neutral or negatively charged when occupied by an electron during electron transport across the barrier via tunneling. The stochastic occupation of traps is governed by random tunneling events of electrons from the left (right) conducting particle to the trap and from the trap to the right (left) conducting particle. Fluctuations in trap occupancy induce local charge fluctuations, which in turn modulate the barrier height. In calculating the noise spectrum associated with trap-occupancy fluctuations, it is typically assumed that the dominant contribution originates from traps whose energy levels coincide with the Fermi level of the conduction electrons in the conducting particle, that the barrier potential can be approximated as rectangular, and that the applied bias is sufficiently small compared to the barrier height. A single discrete trap energy level gives rise to a Lorentzian component in the low-frequency noise spectrum, whereas a distribution of trap energy levels may produce *1/f*-type noise. Therefore, Lorentzian components result from occupancy fluctuations of dominant traps within individual metal-insulator-metal junctures while spatial distribution of traps across all MIM junctions gives rise to *1/f* noise.

This analysis demonstrates that noise spectroscopy provides a sensitive, non-destructive tool for probing microstructural changes in thick-film strain sensors. Variations in the 1/f noise component can be linked to modifications in conducting particle networks and sintered contacts, whereas Lorentzian contributions reveal trap-state dynamics within individual metal–insulator–metal junctions. Monitoring these spectral features allows early

detection of electrically or mechanically induced degradation, facilitating the correlation of processing conditions with microstructural stability and supporting the optimization of sensor design and predictive maintenance strategies. Collectively, these findings highlight the complex dependence of the total noise spectrum on microstructural modifications and trap-state dynamics in electrically stressed and mechanically strained SHM sensors.

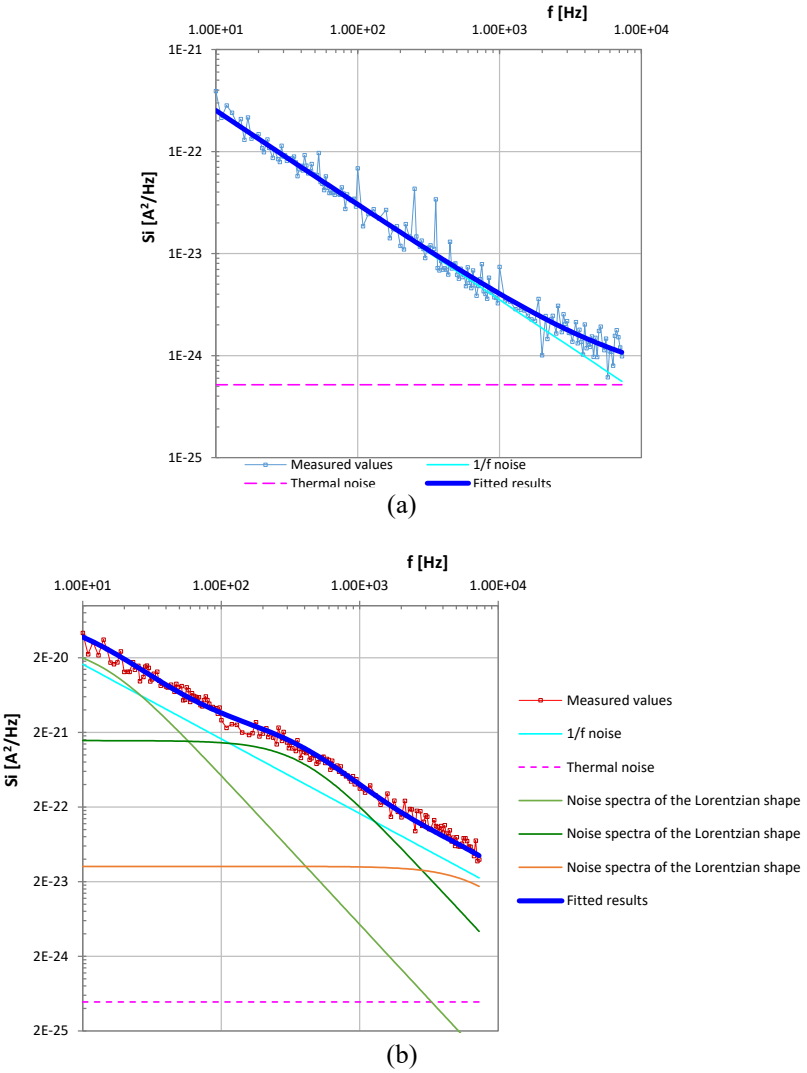

Fig. 6 The experimental results for the current noise spectrum and the fitting results in accordance with Eq. (10) for the thick-film strain sensor with an initial resistance R_2=31.94 kΩ, (a) before and (b) after high-voltage testing (I=0.284 mA), with contributions from different noise sources in the total current noise spectrum

4. CONCLUSION

The experimental investigation demonstrates that thick-film strain sensors based on bismuth lead ruthenate resistive films exhibit significant electrical stability and preserved functional integrity under high-voltage surge conditions. When subjected to a 300 μm substrate deflection and exposed to controlled sequences of high-voltage pulses, the sensors initially exhibited a reduction in resistance, followed by stabilization. This behaviour indicates the sensors' capacity to reach an electrically stable state despite prolonged electrical stress. Throughout the testing procedure, the gauge factor remained unchanged, confirming that the strain sensitivity and electromechanical coupling performance were not compromised. The observed resistance evolution under high-voltage excitation can be attributed to a shift in conduction mechanisms: low-ohmic compositions transitioned from contact-dominated to tunnelling-dominated conduction, while high-ohmic compositions exhibited a reverse trend. These interpretations are supported by parameter p values derived from resistance data and applied within low-frequency noise analysis.

Current noise spectrum measurements revealed a marked increase in *1/f* noise following high-voltage exposure, indicating the formation or activation of additional trap states within the insulating glass matrix. This dominant *1/f* noise component - primarily arising from fluctuations in potential barrier heights and trap occupancy - is accompanied by three Lorentzian components, each associated with localized trap dynamics in individual metal-insulator-metal junctions. While resistance measurements offer insight into macroscopic conduction behaviour, noise spectroscopy proved more sensitive to subtle microstructural changes, particularly those involving conduction path redistribution and trap state dynamics. These results emphasize the critical role of low-frequency noise analysis in assessing the long-term reliability of thick-film sensors, especially in structural health monitoring applications where high-voltage transients are expected.

Future research should address long-term reliability of thick-film strain sensors under continuous surge exposure by combining accelerated testing with noise spectroscopy. Monitoring the evolution of 1/f noise and Lorentzian components during sustained electrical stress would allow early detection of microstructural degradation, such as redistribution of conducting contacts, barrier height variations, and trap-state evolution within metal–insulator–metal junctions. Such studies could establish quantitative links between surge severity, microstructural changes, and sensor lifetime, providing a basis for predictive maintenance strategies and improved sensor design.

Acknowledgement: *The authors are grateful to the Ministry of Science, Technological Development and Innovations of the Republic of Serbia (Contract No. 451-03-136/2025-03/ 200017 and research project No. 200092) for the financial support.*

REFERENCES

[1] S. Hassani, U. Dackermann, "A Systematic Review of Advanced Sensor Technologies for Non-Destructive Testing and Structural Health Monitoring", *Sensors,* vol. 23, p. 2204, 2023.

[2] M. Ju, Z. Dou, J.W. Li, X. Qiu, B. Shen, D. Zhang, F.Z. Yao, W. Gong, K. Wang, "Piezoelectric Materials and Sensors for Structural Health Monitoring: Fundamental Aspects, Current Status and Future Perspectives", *Sensors*, vol. 23, p. 543, 2023.

[3] Z. Deng, M. Huang, N. Wan, J. Zhang, "The Current Development of Structural Health Monitoring for Bridges: A Review", *Buildings*, vol. 13, p. 1360, 2023.

[4] R. Ottermann, E. Müller, M. Keßler, F. Dencker, D. Klaas and M. C. Wurz, "Polymer-Free Batch Production and Application of Metal Foil-Based Thin-Film Strain Gauges", In Proceedings of 2024 IEEE SENSORS, Kobe, Japan, 2024, pp. 1–4.
[5] A. Wilson, P. McMahon, R. Muscat, O. Vargas, P. Vincent, "Thin metal foil sensors", In Proceedings of SPIE, Smart Structures, Devices and Systems III, Adelaide, Australia, 2007, 64140C.
[6] I. Dhingra, G. Kaur, R.S. Kaler, "Design and analysis of fiber Bragg grating sensor to monitor strain and temperature for structural health monitoring", *Opt Quant Electron,* vol. 53, p. 619, 2021.
[7] F.I. Harger Sakiyama, F. Lehmann, H. Garrecht, "Structural health monitoring of concrete structures using fibre-optic-based sensors: a review", *Magazine of Concrete Research*, vol. 73, no. 4, pp. 174–194, 2021.
[8] D.S. Aulakh, S. Bhalla, "3D torsional experimental strain modal analysis for structural health monitoring using piezoelectric sensors", *Measurement*, vol. 180, p. 109476, 2021.
[9] R.K. Langat, W. Deng, E. De Luycker, A. Cantarel, M. Rakotondrabe, "In-situ piezoelectric sensors for structural health monitoring with machine learning integration", *Mechatronics*, vol. 106, p. 103297, 2025.
[10] M. Wen, X. Guan, "Investigation of sensing performances of thick-film resistors sintered on fluorophlogopite glass-ceramic substrates", *Sensors and Actuators A: Physical*, vol. 370, p. 115248, 2024.
[11] S.A.A. Jabir, N.K. Gupta, "Thick-Film Ceramic Strain Sensors for Structural Health Monitoring", *IEEE Transactions on Instrumentation and Measurement*, vol. 60, no. 11, pp. 3669-3676, 2011.
[12] S.A.A. Jabir, N.K. Gupta, "Condition monitoring of the strength and stability of civil structures using thick film ceramic sensors", *Measurement*, vol. 46, no. 7, pp. 2223–2231, 2013.
[13] B. Morten, M. Prudenziati, "Handbook of Sensors and Actuators, Section IV: Sensors for mechanical quantities", ed. M. Prudenziati (Elsevier Science Ltd., Amsterdam, 1994), pp. 189–193, ISBN: 9780444897237.
[14] F. Tondolo, A. Cesetti, E. Matta, A. Quattrone, D. Sabia, "Smart reinforcement steel bars with low-cost MEMS sensors for the structural health monitoring of RC structures", *Construction and Building Materials*, vol. 173, pp. 740–753, 2018.
[15] C.G. Karayannis, C.E. Chalioris, G.M. Angeli, N.A. Papadopoulos, M.J. Favvata, C.P. Providakis, "Experimental damage evaluation of reinforced concrete steel bars using piezoelectric sensors", *Construction and Building Materials*, vol. 105, pp. 227–244, 2016.
[16] S. Munstermann, Y. Feng, W. Bleck, "Influencing parameters on elastic modulus of steels", *Canadian metallurgical quarterly*, vol. 53, no. 3, p. 264, 2014.
[17] S.G. Yousef, J. Rodel, E.R. Fuller Jr., A. Zimmermann, B.S. El-Dasher, "Microcrack Evolution in Alumina Ceramics: Experiment and Simulation", *Journal of the American Ceramic Society*, vol. 88, p. 2809, 2005.
[18] H. Yildirim, O. Sengul, "Modulus of elasticity of substandard and normal concretes", *Construction and building materials*, vol. 25, no. 4, pp. 1645–1652, 2011.
[19] M.M. Jevtić, Z. Stanimirović, I. Mrak, "Low-Frequency Noise in Thick-Film Resistors due to Two-Step Tunneling Process in Insulator Layer of Elemental MIM Cell", *IEEE Transactions on Components, Packaging and Manufacturing Technology-Part A*, vol. 22, no. 1, p. 120, 1999.
[20] C. Grimaldi, T. Maeder, P. Ryser, S Strässler, "A random resistor network model of voltage trimming", *J.Phys.D: Appl.Phys*., vol. 37, pp. 2170–2174, 2004.
[21] I. Mrak, M.M. Jevtić, Zdravko Stanimirović, "Low-frequency Noise in Thick-film Structures Caused by Traps in Glass Barriers", *Microelectronics Reliability*, vol. 38, pp. 1569–1576, 1998.
[22] A. Kusy, A. Szpytma, "On 1/f noise in RuO_2-based thick resistive films", *Solid-State Electronics*, vol. 29. pp. 657–665, 1986.
[23] T. Kleipenning, "On low-frequency noise in tunnel junctions", *Solid-State Electronics*, vol. 25, p. 78, 1982.
[24] M. Prudenziati, B. Morten, A. Masoero, "Excess noise and refiring processes in thick-film resistors", J. Phys. D: Appl. Phys., vol. 14, no. 7, pp. 1355–1362, 1981.